IET Electric Power Applications

Research Article

IET Journals
The Institution of Engineering and Technology

Electromagnetic and thermal analysis and design of a novel-structured surface-mounted permanent magnet motor with high-power-density

ISSN 1751-8660
Received on 8th June 2018
Revised 17th December 2018
Accepted on 28th January 2019
E-First on 5th March 2019
doi: 10.1049/iet-epa.2018.5322
www.ietdl.org

Jae-Gil Lee[1], Han-Kyeol Yeo[2], Hyun-Kyo Jung[1], Tae-Keun Kim[3], Jong-Suk Ro[4] ✉

[1]*Department of Electrical and Computer Engineering, Seoul National University, Seoul, Republic of Korea*
[2]*Research and Development Division, Hyundai Motor Company, Hwaseong, Republic of Korea*
[3]*Intelligent Robotics Research Center, Korea Electronics Technology Institute (KETI), Bucheon, Gyeonggi-do, Republic of Korea*
[4]*School of Electrical and Electronics Engineering, College of ICT Engineering, Chung-Ang University, Seoul, Republic of Korea*
✉ *E-mail: jongsukro@naver.com*

Abstract: A segmented-core (SC) structure has been widely used for high-power-density (HP) motors. However, the SC motor is associated with a number of problems due to the complexity of both the structure and the manufacturing process. To address these issues, a novel structure of a HP motor is proposed, referred to as the ring-coupled segmented-stator (RSS) model here. The proposed RSS can increase the reliability, the stability, and the manufacturability of motor. Furthermore, useful thermal analysis and design flow which take into account the RSS and asymmetric overhang structure of the motor are proposed in this research. The proposed lumped parameter thermal network (LPTN) for the thermal analysis shows a good agreement with experimental data within 9.8% difference. The proposed analysis and design method can be used for the diverse kinds of motor requiring the HP. The usefulness of the proposed RSS motor, the analysis method, and the design method are verified through the experiment in this research.

1 Introduction

Robot is one of the core technologies of what is referred to as the fourth industrial revolution. Recently, the demand for the manufacturing of collaborative robots has increased dramatically [1–4]. Compactness is an important constraint in the manufacturing of a collaborative robot due to the limited work spaces of robots. Hence, a high-power-density (HP) motor is a core component of robots [4].

To increase the power density of such a motor, the segmented-core (SC) structure, which not only increases the coil space factor but also decreases the cogging torque and torque ripple by reducing the slot opening, has become commonly used [5–11]. However, the conventional SC motor, the most widely used type for robots, has the problems such as increases in the cost, decrease in yields, and declines in performance capabilities given the complexity of both the structure and the manufacturing processes [12–16]. To address these problems, a motor with a novel structure is proposed for robots. It is termed as the ring-coupled segmented-stator (RSS) motor here.

To increase the power density, an overhang structure is applied into the proposed RSS motor. The overhang structure makes the height of the magnet and the rotor longer than that of the stator core to utilise the additional magnetic flux and increase the power density [17–19]. In this research, an asymmetric overhang structure is applied into the both end sides of the rotor to utilise the coil end turn and the space for a sensor and a PCB board.

A thermal analysis is essential to increase the reliability and stableness of the motor for a robot. The thermal analysis can be carried out using a numerical method with computational fluid dynamics (CFD) or with an analytic method such as a lumped-parameter thermal network (LPTN) analysis [20–38]. The CFD method can analyse the temperature distribution accurately but requires a considerable amount of time. As repetitive analyses of many models are typically requested during the design of the motor, an accurate and rapid thermal analysis method is required during the motor design process. This can be useful to propose an effective LPTN method because the time required for the analysis as part of the LPTN method is short. Several studies have utilised the LPTN method to undertake a thermal analysis of a motor [20–33, 39]. However, a novel LPTN method is required for the proposed novel RSS surface-mounted permanent magnet (SPM) motor with the asymmetric overhang structure at both ends of the motor. In [29], the convection heat transfer of the external air and the motor was considered by LPTN model of the motor as a horizontal cylinder. The LPTN model of heat transfer by airgap in motor was studied in [27] as the Taylor's rotating cylinder model. The convection phenomena between the stator end and the rotor end and the internal air of enclosed motor was studied in [26]. Specifically, [25] proposed the LPTN model of the convection heat transfer in the motor with symmetric overhang structure. However, there are few studies on the motor with a RSS structure and the asymmetric overhang structure. Hence, a rapid and accurate LPTN analysis method is developed in this research. The rotor saliency is also considered in calculation of convection heat transfer coefficient.

In the conventional motor design process, the current density, which is a significant design constraint, is usually determined based on the experience of the designer without an accurate calculation of the temperature distribution or by a time-consuming thermal analysis via a trial-and-error method. To maximise the power density of the motor, the current density and design conditions must be determined while considering the thermal characteristics of the motor. Therefore, a systematic design method which maximises the power density of the SPM motor considering the temperature constraint is proposed, referred to as the HP design method here.

In this research, two power-level motors for a collaborative robot joint module are designed and manufactured using the proposed components of the RSS motor with the asymmetric overhang structure via the LPTN thermal analysis method, and the HP design method. Through an experiment, the usefulness and validity of the proposed components are confirmed.

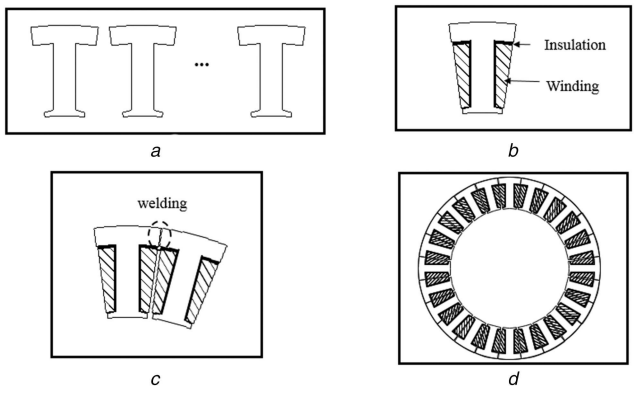

Fig. 1 *Manufacture process using the conventional SC technique.*
(a) Manufacturing T shape sheet and stacking them to make a segmented core, ***(b)*** Winding and insulation of the cores, ***(c)*** Welding segmented cores to manufacture the stator, ***(d)*** Assembled final stator core

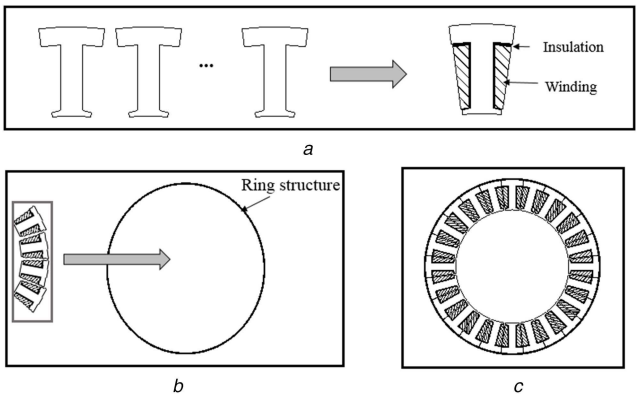

Fig. 2 *Manufacture process using the proposed RSS technique.*
(a) Manufacturing T shape sheet and stacking them to make a segmented core, ***(b)*** Manufacturing a holding ring structure (HRS) made of the structural carbon steel material, S45C and assembling segmented cores and HRS, ***(d)*** Assembled final stator core

Table 1 Comparison between the SC structure and RSS structure

Category	Non-segmented	SC	RSS
torque density	△	◎	◎
manufacturability	◎	○	◎
mechanical coupling intensity	◎	△	○
magnetic distortion	◎	△	◎
cost	◎	△	○

◎: excellent ○: good △: normal

2 Proposal of a novel RSS structure

2.1 Conventional segmented-core structure

The motor for the robot joints requires a HP. The SC structure is widely used in order to increase the power density of the motor through the growth of coil space factor.

As shown in Fig. 1, the SC technique is used to manufacture the stator cores separately, in which the number of the SCs is equal to the number of slots. The coil space factor can be increased by nearly 30% using the SC because the SCs are assembled after the coil is wound in the SCs. In a compact and HP motor for collaborative robot applications, the length of the motor in the axial direction and the yoke in the radial direction are short and the SCs are assembled by the welding. Specifically, the steps of assembling and welding the cores, which are short in the radial direction in the compact space of the cores, increase the degree of mechanical misalignments. Thus, the alignment of the cores in a compact HP motor cannot be guaranteed, causing distortion of the magnetic flux path. Moreover, the magnetic material properties of the core can be distorted by the stress caused by the welding process.

2.2 Proposal of RSS structure

As shown in Fig. 2, the proposed RSS structure does not require a welding process, but it uses an outer ring to align the cores. Accordingly, the risk of misalignment between the SCs in the RSS structure is much lower while also allowing high mechanical and electrical coupling intensity to be retained compared to that in the conventional SC structure. Furthermore, the manufacturing process is simpler and the risk of magnetic deformation is lower compared to the conventional SC structure.

2.3 Proposal of RSS structure

The results of detailed comparison of the SC structure and the RSS structure shown in Table 1 are described below.

2.3.1 Torque density: The torque density of the proposed RSS structure can be slightly lower than that of the conventional SC structure with an identical volume, as the holding ring occupies the volume and thus reduces the effective outer diameter. However, the reduction of the torque density by the ring structure in the RSS is very low.

2.3.2 Manufacturability: The manufacturability of the proposed RSS structure is superior to that of the conventional SC structure because the SC structure requires laser welding to combine the SCs, while the RSS structure does not require a complex manufacturing process. If the number of slots is increased, the time and effort for the laser welding of the SC structure are increased, which reduces the ease of manufacturing.

2.3.3 Mechanical coupling intensity: In the conventional SC structure, the cores are frequently welded with misalignments when the yoke of the stator is thin and the motor is compact. In the case of RSS structure, the outer ring structure fixes and holds the cores stably, maintaining good mechanical alignment and reducing the potential that mechanical distortions will arise.

2.3.4 Magnetic distortion: In the conventional SC structure, the cores retain mechanical stress in the local area because laser welding is used. This causes distortion of the magnetic characteristics of the cores and thus degrades the performance of the motor. On the other hand, the magnetic distortion caused by mechanical stress in the proposed RSS structure is insignificant.

2.3.5 Cost: The RSS structure requires a ring, which can increase its cost somewhat. However, the RSS structure does not need the expensive laser welding process required by the conventional SC structure. Hence, the cost of the RSS structure is much lower than that of the conventional SC structure. Specifically, when the number of slots is increased, the time and effort for the welding in the SC structure are increased, resulting in a cost increase.

3 Proposal of a thermal analysis method

3.1 Thermal analysis of electric machine

The temperature in a motor has a significant effect on the lifetime and performance of the motor. Hence, a thermal analysis is essential in the motor design procedure with an electromagnetic analysis. The CFD and the lumped-parameter thermal network (LPTN) methods are widely used to analyse the thermal characteristics of motors. The accuracy of the CFD is high but the time required for an analysis of a motor makes this process computationally expensive. Hence, the application of the CFD in the motor design process, which requires an analysis of many candidate models, increases the time cost significantly.

To address the time cost problem of the CFD, the LPTN, as described below, is proposed in this research.

3.2 LPTN method

The LPTN method uses a thermal equivalent circuit, which is a simplified model of the complex heat transfer which relies on the

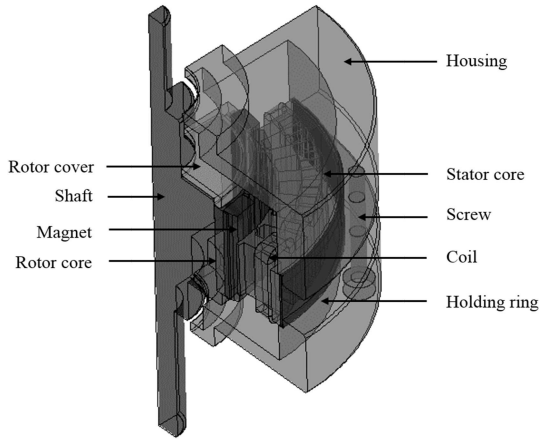

Fig. 3 *Proposed LPTN model for the RSS SPM motor with the asymmetric overhang structure*

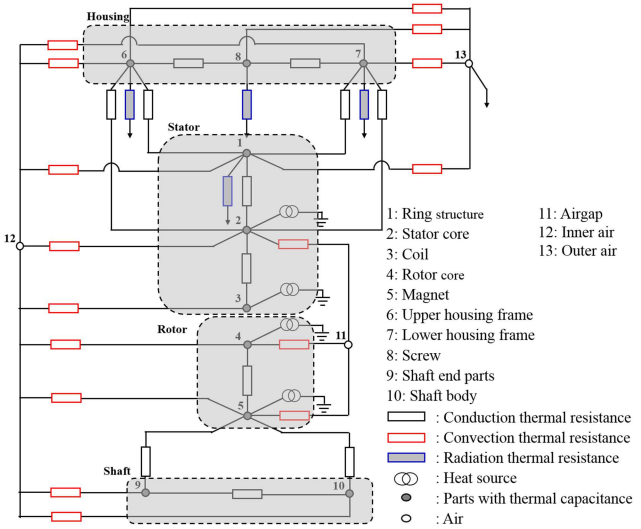

Fig. 4 *Proposed RSS SPM motor with the asymmetric overhang structure*

thermal resistance and the heat source. The thermal resistance is determined based on the degree of heat transfer via conduction, convection, and radiation heat transfer processes.

The LPTN method allows a rapid thermal analysis, but the accuracy of this method depends on the accuracy of the determination of the thermal coefficients. The HP motor commonly uses an overhang structure, and the proposed RSS motor requires a novel heat equivalent model.

Hence, a novel heat equivalent model for analysing the asymmetric overhang structure and the proposed novel structure is proposed in this section.

3.3 Proposed LPTN method

As the LPTN model shown in Fig. 3 is proposed here for a thermal analysis of the proposed RSS SPM motor with an asymmetric overhang structure at both ends of the motor, as shown in Fig. 4. The proposed LPTN model considers the heat transfer under a natural cooling condition. Due to the RSS structure and the asymmetric overhang, it is required to consider the additional heat transfers in the motor. Specifically, the conduction heat transfers are considered between the stator core and the ring structure, and the ring structure and housing. The radiation heat transfer of the ring structure is also considered with its material properties.

Furthermore, the convection heat transfers between the overhang structures and the inner air are independently considered for the different overhang length of top and bottom side of the motor. The heat capacities of components 1 to 10 are considered with each material properties and volumes. The heat capacities of components 11 and 12 are ignored as they represent the air with very small heat capacity value. Finally, the heat capacity of component 13 is assumed to be infinity. The heat sources are the iron loss calculated by a 3-D electromagnetic field analysis and the copper loss estimated by the current and resistance of the coil.

3.3.1 Conduction heat transfer: The resistance values for conduction in Fig. 3 can be calculated by (1), where l_i (m), k_{air} (W/m °C), and A_i (m^2) are the distance between the conductive material, the thermal conductivity of air, and the contact area, respectively. The l_i varies according to the contact condition. A value of 0.03 mm is used in this research for referring to earlier works [25, 28]. In this study, the heat transfer phenomena with contacts among the rotor core, the magnets, the shaft, rotor cover, the stator core, the coils, the ring structure, the housing frame, and the screws are considered as the conduction thermal resistances.

$$R_{\text{cond}} = \frac{l_i}{k_{\text{air}} A_i} \tag{1}$$

3.3.2 Radiation heat transfer: As the cooling condition of the proposed LPTN is natural cooling, radiation heat transfer cannot be ignored. The resistance for radiation between the externally exposed surface of the structure and the ambient air is derived using (2). The radiation heat transfer coefficient is induced by (3), where σ and ε represent Stefan–Boltzmann's constant and the emissivity of the surface, respectively. The surface emissivity values for the housing frame, the screw, and the ring structure are determined based on the earlier research findings [25, 28].

$$R_{\text{rad}} = \frac{1}{h_{\text{rad}} A} \tag{2}$$

$$h_{\text{rad}} = \sigma \varepsilon \frac{(T_s^4 - T_a^4)}{(T_s - T_a)} \tag{3}$$

3.3.3 Convection heat transfer: Convective heat transfer phenomena in the electric motor were classified into three types.

First, the heat transfer between the external air of the motor and the external structure of the motor which is referring to the empirical formula for the horizontal cylinder model in the [29]. Referring the research, the Nusselt number, the thermal conductivity of air, and the diameter of cylinder were used to calculate the heat transfer coefficient.

Second, the heat transfer by airgap was determined referring to Taylor's rotating cylinder model, where the thermal conductivity of air and the axial length of the cylinder were used to calculate the heat transfer coefficient [27].

Finally, the convection phenomena between the stator end and the rotor end and the internal air of the enclosed motor are considered as the heat transfer coefficients, where the angular velocity and outer radius of the rotor are used [25, 26].

In this regard, the proposed LPTN has three types of resistance for convection heat transfer, which can be calculated by (4) and by applying three different values for the convection coefficients h_{conv} (W/m^2 °C). These values are for (i) the outer air and motor structures, (ii) the inner air and motor structures, and (iii) the airgap in the motor.

$$R_{\text{conv}} = \frac{1}{h_{\text{conv}} A} \tag{4}$$

For the proposed RSS SPM motor with the asymmetric overhang structure at both ends of the motor, different values of the convection coefficient h_{conv} for (2) the inner air and motor structures are proposed here, taking into account the following characteristics.

In the overhang structure, the heat transfer amount by convection is augmented as the number of pole is increased. When the gap between the magnets is increased, the heat transfer amount by convection also increases. However, the growth ratio of the heat transfer amount increases rapidly at first and then increases

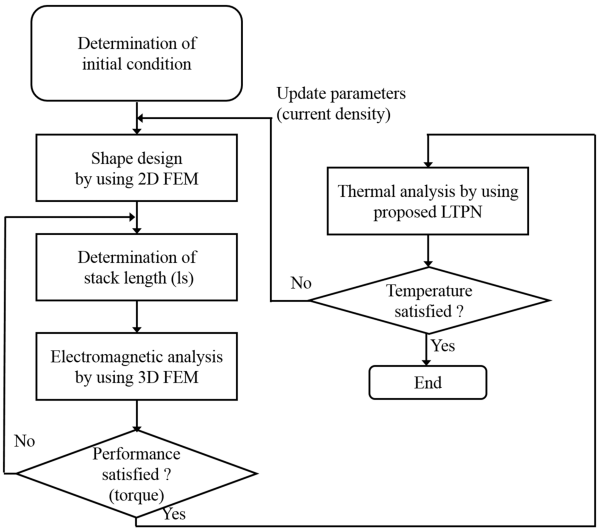

Fig. 5 *Motor design flow using the proposed HP design method*

gradually after the heat transfer becomes saturated with the increased distance of the gap between the magnets.

As the thickness of each magnet is increased, the effect on the heat transfer is also enhanced rapidly. Based on these relationships, the novel coefficient, which we termed the saliency factor k_{sal}, is defined and derived by (5).

$$k_{\text{sal}} = 5.56 \times 10^{7}(n_p m_d^{0.5} m_t^{2.5}) \tag{5}$$

Here, n_p is the number of poles, m_d (m) is the gap between the magnets, and m_t (m) is the thickness of magnet.

To consider the asymmetric overhang structure on both sides of the rotor, (6) and (8) are derived here using the saliency factor k_{sal} and the overhang factor k_{oh}. The $h_{\text{con\_ia1}}$ of (7) represents the convection heat transfer coefficient between the inner air of the motor and the stator end part, and $h_{\text{con\_ia2}}$ of (8) represents the convection heat transfer coefficient between the inner air of the motor and the rotor end part.

$$k_{\text{oh}} = \frac{l_{\text{oh}}}{r_{\text{so}} - r_{\text{ro}}} \tag{6}$$

$$h_{\text{conv\_ia1}} = 6.5 + (5.25 + 3k_{\text{sal}}k_{\text{oh}})^{0.6}(\omega r_{\text{ro}})^{0.6} \tag{7}$$

$$h_{\text{conv\_ia2}} = (16.5 + 5k_{\text{sal}})^{0.65}(\omega r_{\text{ro}})^{0.65} \tag{8}$$

Here, l_{oh} (m) is the length of overhang, ω (rad/s) is the rotational velocity, and r_{ro} (m) is the radius of rotor.

The detailed calculation flow is as follows. At first, we can calculate k_{sal} by (5) with the information of motor shape and specifications. Then, we can simply calculate the overhang factor k_{oh} by (6) with information of motor size. Finally, the heat transfer coefficients represented by (7) and (8) can be calculated by the two factors and the rotational speed of the motor.

4 Proposal of design method

In the design of a typical motor, the current density is determined based on the experience of the designer considering the cooling method or a time-consuming thermal analysis via trial and error. Hence, the conventional process of determining the current density accurately requires much time. To address this issue, a systematic novel design method termed the HP design method is proposed in this research. It is illustrated in Fig. 5. The HP method covers the overall design process, including the determination of the proper current density via thermal and electromagnetic analyses of the motor. Ultimately, the proposed HP method will be useful for the design of a compact HP motor module.

4.1 Step 1 – initial design

In this design stage, the diameter of the stator, the length of the air gap, and the coil space factor are roughly determined taking into account the design requirements and constraints. Subsequently, the number of poles, the number of slots, the diameter of the rotor, and the thickness of the magnet are designed approximately considering the electrical loading, the magnetic loading, and the degree of demagnetisation. The initial value of the current density is determined from earlier cases considering the cooling method.

The magneto-motive force (MMF) can be evaluated approximately considering the current density and the coil space factor. The area of the slot can be roughly determined considering the magnetic flux density.

4.2 Step 2– shape design using 2D-FEM

The required motor performance differs according to the application of the motor. When the motor is applied to the robot, maximisation of the average torque is important because compactness is required for this application. For the medical application of the motor, the stable operation is crucial such as minimised cogging torque and torque ripple.

Considering the required motor performance and the main design objective, the shape of the shoe, the opening of the slot, the pole-pitch of magnet, the shape of the magnet, and other related factors are designed specifically by means of 2D-FEM at this design stage.

4.3 Step 3– determination of stack length

In this design step, the objective is to determine the minimum stack length of the motor considering the required output torque of the motor. The target output torque of the motor must be higher than the required output considering the losses arising from manufacturing uncertainties and the driving losses. Concurrently, an estimation of the additional flux linkage due to the overhang structure must be considered in a test simulation.

If the stack length is determined, the design of the overall shape of the motor can be completely considered. Taking into account the constraints of the voltage and the current, the number of coil turns and the circuit of the motor can be determined together with the coil resistance value.

4.4 Step 4 – electromagnetic analysis using 3D-FEM

At this design stage, the designed motor must be analysed by means of 3D-FEM. The rotor of the proposed motor is thin type with the asymmetric overhang structure. Owing to the asymmetric magnetic flux pattern in the axial direction in the proposed motor, it is essential to ensure a precise characteristic using the 3D-FEM [17].

4.5 Step 5 – performance check

After the 3D-FEM characteristic analysis of the motor, the motor performance which is the requirement of torque, voltage constraint, and current constraint must be checked. If the designed motor performance is insufficient or excessive compared to the target performance, this process then goes to Step 3 for the stack length to be either enlarged or reduced.

4.6 Step 6 – thermal analysis using the proposed LPTN method

With the iron loss, magnet eddy current loss, and the copper loss data, all of which are calculated via an electromagnetic analysis using 3D-FEM, the heat sources can be derived for the analysis of LPTN model. Considering the designed structure of the motor, the final LPTN can be constructed and finally the thermal analysis is conducted.

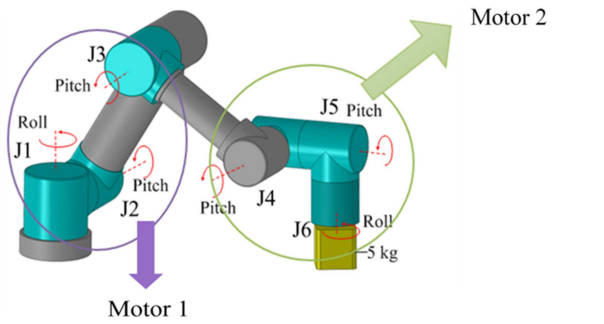

Fig. 6 *Robot joint module with two power levels of 75 and 100 W for motor 1 and motor 2, respectively*

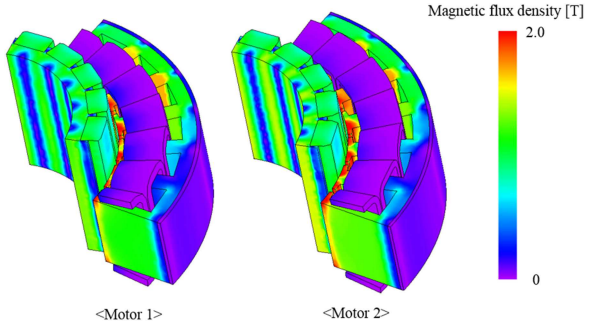

Fig. 7 *Magnetic flux density distribution for designed Motor 1 and 2*

4.7 Step 7 – temperature check

To increase the power density of the motor, the temperature in the motor must be high but within the range of the temperature constraints.

If the estimated saturation temperature in the motor from the thermal analysis of Step 6 is out of objective range considering the temperature constraint, the current density is modified to be higher or lower and the process proceeds to Step 2.

5 Design of motor for robot joint module

In this part, the motor for the robot joint module is designed using the proposed novel RSS and the thermal analysis and the design method. Two different power levels of motors of 75 and 100 W are designed.

5.1 Design requirement

As demonstrated in Fig. 6, the joint arm has six joint modules with the 5 kg payload. The requirements for Module 1 and Module 2 shown in Table 2 are derived considering the required power level of the joints through a dynamic analysis of the manipulator. Taking into account the efficiency of the gear with values of 70–75% and the reduced gear ratios, the rated speed and torque levels are determined as shown in Table 3. The outer diameters for motors 1 and 2 are determined considering the mechanical structure of the joint module. Minimisation of the length in the axial direction to <22 mm is one of the design constraints in this research because compactness is an important point in a cooperative robot joint module with several sensor components.

5.2 Design result

The design result of the motor for the robot joint module using the proposed RSS structure and the analysis and design method is described below.

The 20-pole and 24-slot is selected considering the power density, the switching frequency of the inverter, ease of manufacturability, winding factor, and other pertinent factors.

One of the design objectives is to maximise the power density in the continuous operation mode. Moreover, the temperature of the housing frame should be <70°C for the reliability and safety of robot module. In this research, the target temperature of the housing frame is set to 60°C considering a 15% margin. The design is carried out using the proposed HP design method while checking the estimated temperature of the housing frame to derive the HP motor with the optimal current density in the coil.

The height of the asymmetric overhang structure is determined while taking into account the height of the end turn of the coil as well as the sensor system.

As shown in Fig. 7, the magnetic flux density in the designed motors is evenly distributed and it is confirmed that the operating point is not at extremely saturated level. As demonstrated in Table 4, the THD of the designed motor is <2% and the cogging torque is <1.5% as compared to the rated torque, thus satisfying the design requirements. The losses are also represented in Table 5 including the iron loss, the copper loss, and the magnet eddy current loss. The loss information is used for the heat sources in the LPTN analysis.

The copper loss at an ambient temperature of the designed motor is greater than the iron loss that, as the rotational speed of motor is not high and the current density is maximised within the temperature constraint. The calculated losses are used for the heat sources in the LPTN method. By utilising the derived heat transfer coefficients shown in Table 6 for use with the LPTN method, the estimation of the saturation temperature in motor and the HP design can be carried out.

Table 2 Requirement for the module 1 and module 2

Items	Module 1 (for joint 1,2, 3)	Module 2 (for joint 4,5, 6)
rated speed, rpm	25	20
avg. load torque, N·m	20	34
max. load torque, N·m	35	58

Table 3 Design requirements for motor 1 and 2

Items	Motor 1	Motor 2
rating speed, rpm	2000	
rating power, W	75	100
rating torque, N·m	0.36	0.475
max. torque, N·m	0.63	1.07
outer diameter, mm	58	70
input voltage, V	48	
cont. current limit, Arms	5	
max. current limit, Arms	10	
cooling type	self-cooled	
temperature constraint, °C	70 (housing frame)	
core material	S08	
magnet remanence, T	1.32	

Table 4 Performance of the designed motors

Items	Motor 1	Motor 2
EMF magnitude, V at 2000 rpm	30.04	31.39
back EMF THD, %	1.94	2.07
cogging torque, mN·m	5.47	5.62
efficiency, %	88.5	87.6

Table 5 Loss data of the designed motors

Items	Motor 1	Motor 2	Motor 2
copper loss at 20°C, W	7.26	6.15	6.15
rotor Iron loss, W	0.002	0.013	0.013
stator Iron loss, W	2.49	4.43	4.43
eddy current loss in magnets, W	0.001	0.001	87.6

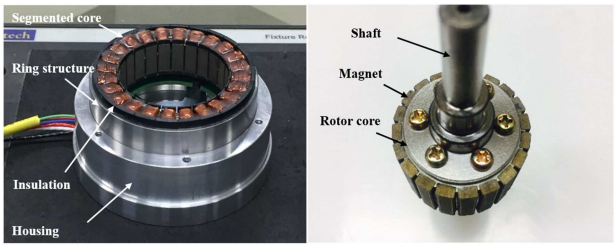

Fig. 8 *Prototype of the RSS SPM motor for robot joint module*
(a) Stator, ***(b)*** Rotor

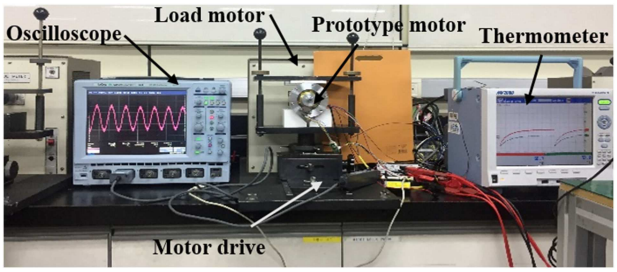

Fig. 9 *Experimental system*

6 Experimental data of the RSS SPM motor

6.1 Prototype of RSS SPM motor with the asymmetric overhang

As shown in Fig. 8, a carbon-steel ring is installed such that it encircles the stator with the asymmetric overhang structure. The experiment was carried out in a laboratory at an ambient temperature of around 20°C, as shown in Fig. 9.

6.2 Result of EMF

The electromotive force was measured under a no-load condition at 1000 rpm. The measured peak value of the phase EMF of 75 W motor and 100 W motor was, respectively, 29.72 and 30.77 V under 2.1% difference with the estimated data in Table 4.

6.3 Result of efficiency

The efficiency rates of the 75 W motor and the 100 W motor were 85.4 and 83.1% in the experiment, respectively. The corresponding calculated efficiencies of the 75 W motor and the 100 W motor were 88.5, and 87.6%, showing some difference from the experimental data. The difference between the experimental data and the calculated data may be due to the coupling problem between the motor and the load, distortion of the current source, and/or a phase imbalances which arose during the experiment.

6.4 Result of temperature rise

The temperature check in the coil is very important to guarantee the safe and secure operation of the motors. Moreover, we need to check the one of design requirement which is within 60°C of housing temperature as described in Section 5.2. In this regard, we installed the thermocouples in stator coil and housing surface of the motors. Then, we finally compared the experimental data and the analysis results by the proposed LPTN.

As shown in Fig. 10 and Table 7, the measured temperature data in motor 1 and motor 2 are well-fitted with regard to all the calculated data using the proposed temperature analysis method, i.e. the LPTN method <10% difference. Hence, it is confirmed that the proposed analytic method, LPTN, is rapid and accurate.

Moreover, motor1 and motor 2, as designed by the proposed analysis and design methods, operate within the maximum constraint temperature 60°C in the housing frame with a HP method. This confirms that the proposed analysis and design method will be useful in the analysis and design of a HP motor.

Table 6 Convection heat transfer coefficient for the designed motor

Items	Motor 1	Motor 2
h_{conv_ia11}, W/m^2 °C	15.28	14.64
h_{conv_ia12}, W/m^2 °C	21.68	21.62
h_{conv_ia21}, W/m^2 °C	13.79	13.69
h_{conv_ia22}, W/m^2 °C	21.68	21.62

h_{conv_ia11}: convection heat transfer coefficient between the inner air of motor and the stator end part of top side.

h_{conv_ia12}: convection heat transfer coefficient between the inner air of motor and the rotor end part of top side.

h_{conv_ia21}: convection heat transfer coefficient between the inner air of motor and the stator end part of bottom side.

h_{conv_ia22}: convection heat transfer coefficient between the inner air of motor and the rotor end part of bottom side.

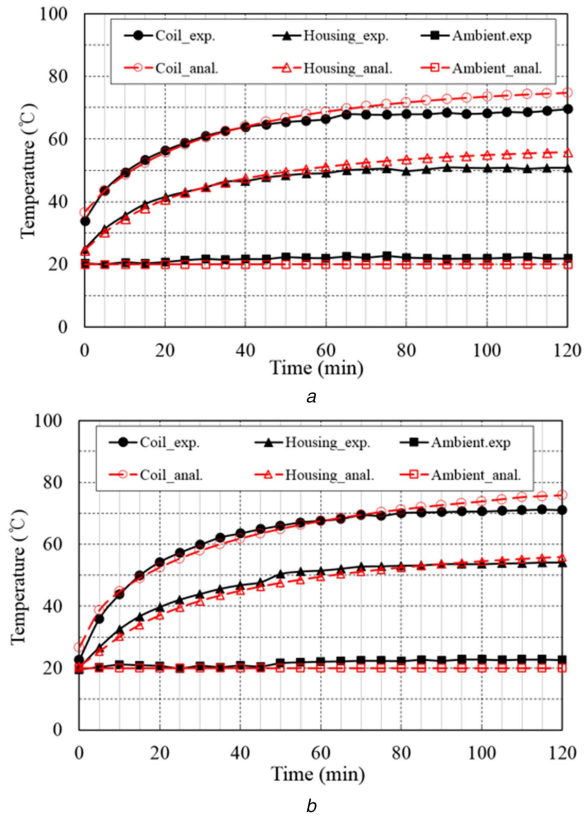

Fig. 10 *Temperature comparison of motor 1 and 2 in the continuous operating condition between the experimental data and the calculated data by the proposed LPTN method*
(a) Motor 1, ***(b)*** Motor 2

Table 7 Temperature comparison between experimental and calculated data by using the proposed LPTN method for motor 1 and motor2 in the housing and coil

	Measuring point	Temperature, °C	
		LPTN	Experiment
Motor 1	coil	74.8	69.5
	housing	55.8	50.8
Motor 2	coil	75.9	71.0
	housing	56.1	54.1

Saturation temperature was measured after 2 h operation at rated condition.

7 Conclusion

Due to the increasing demand for robots, compact and HP motors are required. However, the conventional SC motor for robots has several shortcomings in terms of the cost, yield, and performance due to the complex structure and manufacturing process required.

Hence, the significance of this paper is its proposal of a novel structure of a HP RSS motor of which the cost, yield, and performance are superior to those of a conventional SC motor.

A thermal analysis of a motor for use with robots is required to increase the reliability and stability. Therefore, it is noteworthy that a rapid and accurate LPTN analysis method for the proposed RSS motor with an asymmetric overhang structure is proposed in this research.

A systematic design method considering the temperature distribution in a motor has yet to be studied in depth. Hence, an important contribution here is that a useful HP design method which maximises the power density of a SPM motor considering the temperature rise as a constraint is proposed.

Significantly, the proposed RSS structure, the LPTN method, and HP design method are widely applicable to many of the types of motors as well.

8 Acknowledgments

This research was supported by X-mind Corps program of National Research Foundation of Korea (NRF) funded by the Ministry of Science, ICT & Future Planning (2017H1D8A1030599), and the Engineering Development Research Centre through the Ministry of Trade, Industry and Energy under Grant N0000990.

9 References

[1] Inoue, T., Yamamoto, S., Miyata, R., *et al.*: 'A robotic joint design by agonist and antagonist arrangement with twisting small-diameter round-belts'. IEEE Int. Conf. on Intelligent Robots and System, Hamburg, Germany, 2015

[2] Seifer, D. F., Mataric, M.: 'Defining socially assistive robotics'. IEEE Int. Conf. on Rehabilitation Robotics, Chicago, IL, USA, 2005, pp. 465–468

[3] Rahman, S.M.M.: 'A novel variable impedance compact compliant series elastic actuator for human-friendly soft robotics applications'. IEEE Int. Symp. On Robot and Human Interactive Communication, Paris, France, 2012, pp. 19–24

[4] Seo, J. M.: 'Design of surface-mounted permanent magnet motor for robot considering dynamic load characteristics', Ph.D. dissertation, Dep. Electric. and Com. Eng., Seoul National Univ., Seoul, Korea, 2016

[5] Momen, M. F., Datta, S.: 'Analysis of flux leakage in a segmented core brushless permanent magnet motor', *IEEE Trans. Energy Convers.*, 2009, **24**, (1), pp. 77–81

[6] Akita, H., Nakahara, Y., Miyake, N., *et al.*: 'New core structure and manufacturing method for high efficiency of permanent magnet motors'. Industry Application Conf. Annual Meeting, Salt Lake City, UT, USA, 2003

[7] Bianchi, N., Bolognani, S., Frare, P.: 'Design criteria for high-efficiency SPM synchronous motors', *IEEE Trans. Energy Convers.*, 2006, **21**, (2), pp. 396–404

[8] Aghdam, S. R. M., Feyzi, M. R., Bianchi, N.: 'Design and analysis of a novel-high-torque stator-segmented SRM', *IEEE Trans. Ind. Electron.*, 2016, **63**, (3), pp. 1458–1466

[9] Shen, J. X., Cai, S., Shuai Cao, J. Y., *et al.*: 'Cogging torque in SPM machine with segmented stator', *Int. J. Comput. Math. Electr. Electron. Eng.*, 2016, **35**, (2), pp. 376–395

[10] Zhu, Z. Q., Chen, J. T., Wu, L. J., *et al.*: 'Influence of stator asymmetry on cogging torque of permanent magnet brushless machines', *IEEE Trans. Magn.*, 2008, **44**, (11), pp. 3851–3854

[11] Zhu, Z. Q., Howe, D.: 'Influence of design parameters on cogging torque in permanent magnet machines', *IEEE Trans. Energy Convers.*, 2000, **15**, (4), pp. 407–412

[12] Zhu, Z. Q., Azar, Z., Ombach, G.: 'Influence of additional air gaps between stator segments on cogging torque of permanent-magnet machines having modular stators', *IEEE Trans. Magn.*, 2012, **48**, (6), pp. 2049–2055

[13] Lee, T. Y., Seo, M. K., Kim, Y. J., *et al.*: 'Cogging torque of surface-mounted permanent magnet synchronous motor according to segmented-stator core effect'. Int. Conf. on Electromagnetic Field Computation, Lausanne, Switzerland, 2016

[14] Jing, L. B., Liu, L., Qu, R. H., *et al.*: 'A novel method of reducing the cogging torque in SPM machine with segmented stator', *J. Electr. Eng. Technol.*, 2017, **12**, (2), pp. 718–725

[15] Nakazaki, O., Kai, Y., Todaka, T., *et al.*: 'Iron loss properties of a practical rotating machine stator core at each manufacturing stage, *Int. J. Appl. Electromagn. Mech.*, 2010, **33**, (1–2), pp. 79–86

[16] Jeong, K., Ren, Z., Kwon, O., *et al.*: 'Measurement and comparison of iron loss in bonded- and embossed-type segmented stator cores for IPMSM', *J. Electr. Eng. Technol.*, 2014, **9**, (6), pp. 2013–2018

[17] Kim, K. C., Koo, D. H., Lee, J.: 'The study on the overhang coefficient for permanent magnet machine by experiment design method', *IEEE Trans. Magn.*, 2007, **43**, (6), pp. 2483–2485

[18] Hwang, K. Y., Lin, H., Rhyu, S. H., *et al.*: 'A study on the novel coefficient modeling for a skewed permanent magnet and overhang structure for optimal design of brushless DC motor', *IEEE Trans. Magn.*, 2012, **48**, (5), pp. 1918–1923

[19] Kang, G. H., Son, Y. D., Kim, G. T.: 'The noise and vibration analysis of BLDC motor due to asymmetrical permanent magnet overhang effects', *IEEE Trans. Ind. Appl.*, 2008, **44**, (5), pp. 1569–1577

[20] Cengel, Y.A.: '*Heat transfer: a practical approach*' (McGraw-Hill, New York, NY, USA, 2003, 2nd edn.)

[21] Mellor, P. H., Roberts, D. R., Turner, D.: 'Lumped parameter thermal model for electrical machines of TEFC design', *IEE Proc., Electr. Power Appl.*, 1991, **138**, (5), pp. 205–218

[22] Lee, B. H., Kim, K. S., Jung, J. W., *et al.*: 'Temperature estimation of IPMSM using thermal equivalent circuit', *IEEE Trans. Magn.*, 2012, **48**, (11), pp. 2949–2952

[23] Sarkara, D., Bhattacharya, N. K., Naskar, A. K.: 'Computation of thermal condition in an induction motor during reactor starting', *Int. J. Electr. Power Energy Syst.*, 2013, **44**, (1), pp. 938–948

[24] Kefalas, T. D., Kladas, A. G.: 'Thermal investigation of permanent-magnet synchronous motor for aerospace applications', *IEEE Trans. Ind. Electron.*, 2014, **61**, (8), pp. 4404–4411

[25] Yeo, H. K., Park, H. J., Seo, J. M., *et al.*: 'Electromagnetic and thermal analysis of a surface-mounted permanent-magnet motor with overhang structure', *IEEE Trans. Magn.*, 2017, **53**, (6), Article ID: 8203304

[26] Kylander, G.: 'Thermal modelling of small cage induction motors'. Ph.D. dissertation, School of Electrical and Computer Engineering Chalmers University of Technology, Gothenburg, Sweden, 1995

[27] Bousbaine, A.: 'An investigation into the thermal modelling of induction motors'. Ph.D. dissertation, Department of Electronics, and Electric Engineering University of Sheffield, Sheffield, UK, 1993

[28] Staton, D., Boglietti, A., Cavagnino, A.: 'Solving the more difficult aspects of electric motor thermal analysis in small and medium size industrial induction motors', *IEEE Trans. Energy Convers.*, 2005, **20**, (3), pp. 620–628

[29] Cengel, Y. A.: '*Heat transfer: a practical approach*' (McGraw-Hill, New York, NY, USA, 2002, 2nd end.)

[30] Mugglestone, J., Pickering, S. J., Lampard, D.: 'Effect of geometric changes on the flow and heat transfer in the end region of a TEFC induction motor'. Int. Conf. on Electrical Machines and Drives, Canterbury, UK, Sep. 1999

[31] Boglietti, A., Cavagnino, A., Staton, D.: 'Determination of critical parameters in electrical machine thermal models', *IEEE Trans. Ind. Appl.*, 2008, **44**, (4), pp. 1150–1159

[32] Boglietti, A., Cavagnino, A., Lazzari, M., *et al.*: 'A simplified thermal model for variable-speed self-cooled industrial induction motor', *IEEE Trans. Ind. Appl.*, 2003, **39**, (4), pp. 945–952

[33] Staton, D., Cavagnino, A.: 'Convection heat transfer and flow calculations suitable for electric machines thermal models', *IEEE Trans. Ind. Electron.*, 2008, **55**, (10), pp. 3509–3516

[34] Seo, J. H.: 'Thermal analysis and optimal design of interior permanent magnet motors for vehicle applications'. PhD dissertation, Department Electric and Computer Engineering, Seoul National Univ., Seoul, Korea, 2010

[35] Marignetti, F., Colli, V. D., Coia, Y.: 'Design of axial flux PM synchronous machines through 3-D coupled electromagnetic thermal and fluid-dynamical finite-element analysis', *IEEE Trans. Ind. Electron.*, 2008, **55**, (10), pp. 3591–3601

[36] Micallef, C., Pickering, S. J., Simmons, K. A., *et al.*: 'Improved cooling in the end region of a strip-wound totally enclosed fan-cooled induction electric machine', *IEEE Trans. Ind. Electron.*, 2008, **55**, (10), pp. 3517–3524

[37] Jungreuthmayer, C., Bäuml, T., Winter, O., *et al.*: 'A detailed heat and fluid flow analysis of an internal permanent magnet synchronous machine by means of computational fluid dynamics', *IEEE Trans. Ind. Electron.*, 2012, **59**, (12), pp. 4568–4578

[38] Popescu, M., Dorrel, D. G., Alberti, L., *et al.*: 'Thermal analysis of a duplex three-phase induction motor under fault operating conditions', *IEEE Trans. Ind. Appl.*, 2002, **49**, (4), pp. 1523–1530

[39] Chun, Y. D., Lee, J., Wakao, S.: 'Overhang effect analysis of brushless DC motor by 3-D equivalent magnetic circuit network method', *IEEE Trans. Magn.*, 2003, **39**, (3), pp. 1610–1613